Available online at www.sciencedirect.com

SciVerse ScienceDirect

Ceramics International 39 (2013) 4529–4537

CERAMICS INTERNATIONAL

www.elsevier.com/locate/ceramint

# Microstructure and mechanical properties of MgO–C refractories containing expanded graphite

Tianbin Zhu, Yawei Li*, Shengli Jin, Shaobai Sang, Qinghu Wang, Lei Zhao, Yuanbing Li, Shujing Li

*The Key State Laboratory Breeding Base of Refractories and Ceramics, Wuhan University of Science and Technology, Wuhan 430081, PR China*

Received 23 October 2012; received in revised form 9 November 2012; accepted 16 November 2012
Available online 27 November 2012

**Abstract**

MgO–C refractories containing expanded graphite particles (EGs) and Al, Si additives were prepared. The EGs were prepared firstly by exfoliating commercial expandable graphite. Then, the composite powder containing EGs was obtained by mixing EGs and magnesia powder and incorporated into MgO–C refractories. The microstructure and mechanical properties of all the MgO–C refractories obtained were investigated by X-ray diffraction (XRD), scanning electron microscopy (SEM) coupled with energy dispersive X-ray spectroscopy (EDS), three-point bending and thermal shock tests. The results showed that EGs affected the microstructural evolution of MgO–C refractories. Much more interlocking aluminum carbides and nitride phases formed in the matrix of the specimen containing EGs because of their higher activity compared to flaky graphite. Also, EGs had a positive influence on the mechanical properties of MgO–C refractories. MgO–C specimens containing EGs had much higher cold modulus of rupture and better toughness compared to the specimens containing only flaky graphite; furthermore, the thermal shock resistance of MgO–C refractories was improved with the addition of EGs. It was suggested that EGs and in-situ formed ceramic phases in the matrix had a strengthening and toughening effect on MgO–C refractories.


*Keywords:* C. Mechanical properties; Microstructure; EGs; MgO–C refractories

## 1. Introduction

Many efforts have been made to develop low carbon refractories for the production of low carbon and ultra-low carbon steels. Approaches used to prepare low carbon refractories with outstanding mechanical and thermal properties included the addition of micro-/nano-powders and the incorporation of one dimensional nanosized carbon. For instance, carbon black has been used widely in recent years to make low carbon containing refractories [1–11]. Bag et al. [12] reported that the addition of 0.9 wt% nanosized carbon in combination with 3 wt% flaky graphite gave the best properties in their low carbon refractories. Carbon nanofibers (CNFs) or carbon nanotubes (CNTs) have also been investigated for their use as carbon sources for low carbon refractories due to their unique thermal, mechanical and chemical properties [13,14]. Matsuo et al. [15] reported an enhancement of 2.2 times in strength for the MgO–C specimen containing 0.4 wt% CNFs compared to that containing no CNFs, owing to the crack arresting effect of CNFs. Also, Luo et al. [16] found that better mechanical properties can be obtained in $Al_2O_3$–C refractories when 0.05 wt% CNTs was added. Roungos and Aneziris [17] also reported that adding of CNTs in combination with aluminum nanosheets in $Al_2O_3$–C refractories led to superior thermal shock resistance.

Recently, another new type of nanosized carbon, graphene or graphite oxide nanosheets (GONs), was investigated for use as a reinforced phase for the polymer matrix and ceramic matrix composites owing to its excellent mechanical, thermal and electrochemical properties [18–22]. For example, Wang et al. [23] obtained a fracture toughness value of 5.21 MPa $m^{1/2}$ for the graphene nanosheets/alumina composites,

*Corresponding author. Tel.: +86 27 68862188; fax: +86 27 68862018.
*E-mail address:* liyawei@wust.edu.cn (Y. Li).

0272-8842/$ - see front matter © 2012 Elsevier Ltd and Techna Group S.r.l. All rights reserved.
http://dx.doi.org/10.1016/j.ceramint.2012.11.049

which was 53% higher than that for pure alumina (3.40 MPa $m^{1/2}$). In previous work, GONs were incorporated into MgO–C refractories as new carbon source to improve the mechanical and thermo-mechanical properties owing to their morphology and high activity [24]. In fact, the mechanical and thermo-mechanical properties of carbon containing refractories can be influenced by the amount and morphology of in situ formed ceramics in the matrix [25–30]. Hayashi et al. [31] also found that superior toughening behavior was obtained in MgO–C refractories containing expanded graphite compared to the specimens containing flaky graphite. In the present work, expanded graphite (EG) was used as carbon source to partially replace flaky graphite in MgO–C refractories in order to study the effect of its addition on the microstructure and mechanical and thermo-mechanical properties, and further elucidate the strengthening and toughening mechanisms of this kind of material.

## 2. Experimental

### 2.1. Preparation of MgO–EGs and MgO–GONs composite powder

The expanded graphite (EG) was prepared by exfoliating commercial expandable graphite (50 mesh, 96 wt% fixed carbon, Qingdao, China) in a microwave oven (MM721AAU-PW, Midea, 700 w) for 20 s. In order to distribute the EGs homogeneously in magnesia powders, the as-prepared EGs and MgO powders (~45 μm, 98 wt%, Dashiqiao, China) were mixed for 3 h in a polyurethane bottle rotating at a speed of 400 rev/min with corundum balls as the abrasive media; the mixing ratio of magnesia powder to EG was 100:2, and the mass ratio of corundum balls to the powder mixtures was 1:1. The composite powder obtained was designated as MgO–EGs. It was further ball-milled at a rotating speed of 400 rev/min for 7 h in a planetary ball mill using N-methyl pyrrole (NMP) as the disperse media, which was followed by drying at 60 °C for 120 h and then dry-grinding into fine powders; the powder obtained at this stage was designated as MgO–GONs.

### 2.2. Preparation of MgO–C refractory specimens

The raw materials used for preparing the batch compositions of the MgO–C refractories were fused magnesia (3–1 mm, 1–0.5 mm, 0.5–0 mm and < 45 μm, 98 wt% MgO, Dashiqiao, China), silicon powder (< 45 μm, 98 wt% Si, Anyang, China), aluminum powder (< 45 μm, 98 wt% Al, Xinxiang, China), flaky graphite (FG, < 74 μm, 97.5 wt% fixed carbon, Qingdao, China), as-obtained MgO–EGs and MgO–GONs composite powders. Thermosetting phenolic resins, one in liquid form (36 wt% of carbon yield, Zibo, China) and one in powder form (55 wt% carbon yield, Zibo, China) were used as binders. The batch compositions investigated are given in Table 1. All the batches were mixed for 30 min in a mixer with a rotating speed of 80–100 rev/min. After kneading, bar shaped specimens (140 mm × 25 mm × 25 mm) were prepared by cold pressing at 150 MPa and then cured at 200 °C for 24 h. Finally, the as-prepared specimens were fired at 1000 °C and 1400 °C for 3 h in a sagger filled with coke grit; the heating rate used was 5 °C/min.

Table 1
Batches composition of MgO–C refractory specimens.

| Ingredient (wt%) | S-FG | S-GONs | S-EG |
|---|---|---|---|
| Fused magnesia aggregate | 70 | 70 | 70 |
| Magnesia powder | 22 | 12 | 12 |
| Flaky graphite (FG) | 5 | 4.8 | 4.8 |
| MgO–GONs | | 10.2 | |
| MgO–EGs | | | 10.2 |
| Silicon powder | 1 | 1 | 1 |
| Metallic aluminum | 2 | 2 | 2 |
| Phenolic resin powder | +0.4 | +0.4 | +0.4 |
| Liquid phenolic resin | +4 | +4 | +4 |

### 2.3. Tests and characterization methods

The bulk density (BD) and apparent porosity (AP) of the MgO–C refractory specimens were measured according to Archimedes' Principle with kerosene as the medium. Mechanical properties including cold modulus of rupture (CMOR) and flexural modulus (FM) were measured by the three-point bending test at ambient temperature with a span of 100 mm and a loading rate of 0.5 mm/min using an electronic digital control system (EDC 120, DOLI Company, Germany). The force–displacement curve of each refractory specimen was recorded simultaneously during the test. The phase composition and microstructure of the specimens were analyzed by means of X-ray diffraction (XRD) (X'Pert Pro, Philips, Eindhoven, The Netherlands; using Ni filtered, Cu $K_\alpha$ radiation at a scanning rate of 2°/min and a temperature of 289 K (16 °C)), and field emission scanning electron microscopy (SEM) (Nova 400 Nano FESEM, FEI Co., Philips, Eindhoven, The Netherlands) coupled with energy dispersive X-ray spectroscopy (EDS) (EDAX, Phoenix, Philips, Eindhoven, The Netherlands).

The thermal shock resistance of the specimens fired at 1400 °C was tested by firstly heating the specimens in a coke bed to 1100 °C with a heating rate of 5 °C/min and then soaking at this temperature for 30 min, which was followed by quickly quenching into an oil bath; the purpose of using an oil bath instead of water bath was to prevent oxidation and hydration of the specimens. This cycle was repeated 5 times. After 5 thermal shock cycles, the mechanical properties of the specimens were assessed by the three-point bending test. The residual strength ratio of CMOR was calculated by the change in CMOR before and after the thermal shocks, i.e. the residual strength ratio of $CMOR = 100CMOR_{TS}/CMOR$, where CMOR and $CMOR_{TS}$ were the CMOR before and after 5 thermal shock cycles, respectively.

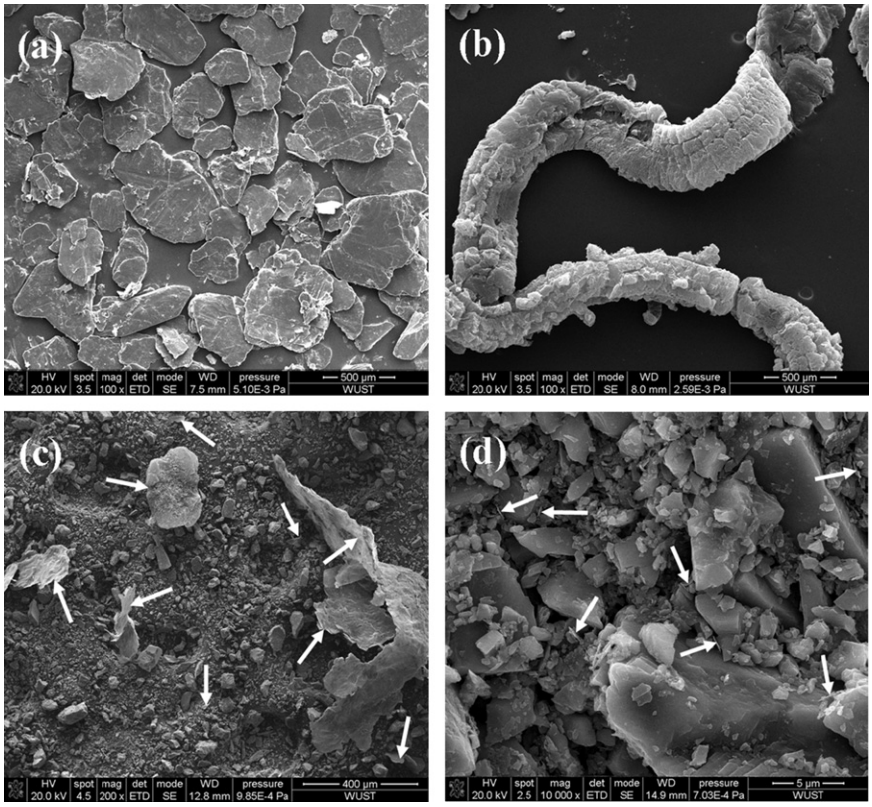


Fig. 1. SEM images of different types of carbon: (a) FG, (b) EG, (c) MgO–EGs and (d) MgO–GONs.

## 3. Results and discussion

### 3.1. SEM images of FG, EG and GONs

The original micrographs of FG and EG are shown in Fig. 1a and b, respectively. FG exhibits a laminar structure, while EG is a worm-like structure with large amount of multi-pores [24,32,33]. EGs exfoliated by mixing and ball milling were fragmented and distributed evenly in magnesia powders, as indicated in Fig. 1c and d. The difference between the composite powders MgO–EGs and MgO–GONs was that graphite particles with different sizes distributed homogeneously in MgO–EGs powders. For example, MgO–EGs powders contained both small GONs 1–5 μm in size and large graphite flake of several hundred microns in size, while the size of graphite flake in the MgO–GONs powders was 1–3 μm.

### 3.2. The phase composition and microstructure of MgO–C refractory specimens

Fig. 2 shows XRD patterns of MgO–C refractory specimens fired at 1000 °C and 1400 °C. It is evident that the spinel phase appeared together with periclase, graphite and silicon phases in all the specimens fired at 1000 °C (Fig. 2a), whereas AlN and SiC phases formed but Si disappeared in the specimens firing at 1400 °C (Fig. 2b). The Al carbides such as $Al_4C_3$ and $Al_2OC$ phases were not detected in MgO–C specimens because their content was too low to be detected by XRD, which was also the case as discussed in the previous work [17,24,27].

SEM micrographs showing the ruptured surface of MgO–C refractory specimens subjected to treatment at different temperatures are presented in Figs. 3–5. For the compositions cured at 200 °C (Fig. 3), much more EGs were torn off from the matrix of the specimen S-EG while flaky graphite was almost intact in the specimens S-FG and S-GONs. In all specimens fired at 1000 °C (Fig. 4), the in situ formed fibrous structures (identified as Al carbides by EDS analysis) and cubic crystalline particles (confirmed as magnesia–alumina spinel by XRD and EDS) appeared in the matrix where aluminum particles were originally located, which was consistent with the observations of previous studies [27,34]. Furthermore, these phases were much more easily found in the matrix of MgO–C refractories containing EGs and GONs. For the specimens fired at 1400 °C (Fig. 5), the microstructural difference in specimens of the three different compositions resulted from the amount and distribution of lamellate grains, which were confirmed as AlN by XRD and EDS. It can be seen obviously that the amount of AlN formed in S-FG (Fig. 5a and b) was less than in the specimens S-EG and S-GONs (Fig. 5c–f), which contained EGs and GONs, respectively. The specimen S-EG contained the highest amount of AlN with interlocking grains distributed in the pores as well as in the matrix (Fig. 5e and f). In addition, some of the EGs were pulled out at the local positions in the specimen S-EG (Fig. 5g), implying that the specimen S-EG might have higher toughness.

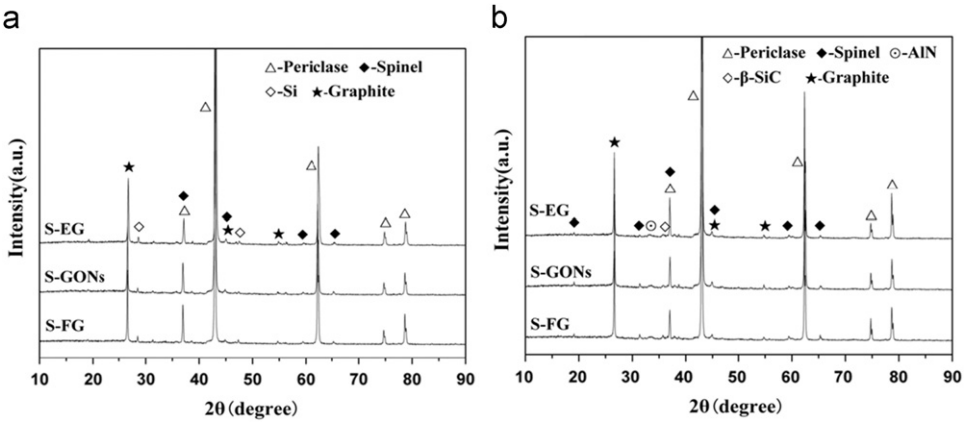


Fig. 2. XRD patterns of MgO–C refractory specimens fired at 1000 °C (a) and 1400 °C (b).

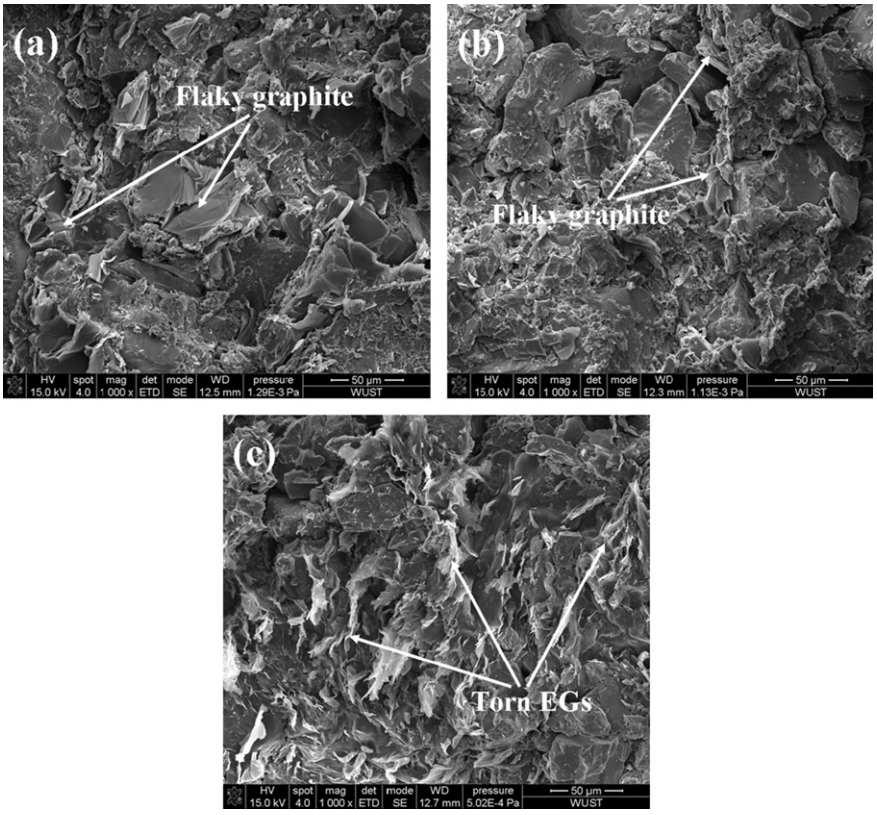


Fig. 3. SEM micrographs of MgO–C refractory specimens (a) S-FG, (b) S-GONs and (c) S-EG cured at 200 °C.

### 3.3. The mechanical properties of MgO–C refractory specimens

Mechanical properties including CMOR and FM of MgO–C refractories were measured using the three-point bending test at room temperature, and the results are presented in Table 2. For the different compositions cured at 200 °C, the specimen S-FG had the lowest CMOR and FM values (20.33 MPa and 5854 MPa, respectively) and the specimen S-EG had the highest CMOR and FM values (28.32 MPa and 6515 MPa, respectively). The high CMOR and FM values of the specimen S-EG may be attributed to the extent of close packing of the specimens (Table 3) and the toughening effect of large sized EGs via a pull out mechanism (Fig. 3c). Among the specimens fired at 1000 °C, the specimen S-GONs had the highest CMOR and FM values, which were 7.72 MPa and 2261 MPa, respectively. CMOR and FM increased simultaneously in all the specimens as the firing temperature was increased from 1000 °C to 1400 °C. Meanwhile, the specimens containing EGs and GONs (S-EG and S-GONs) had greater CMOR and FM values than the specimen containing only

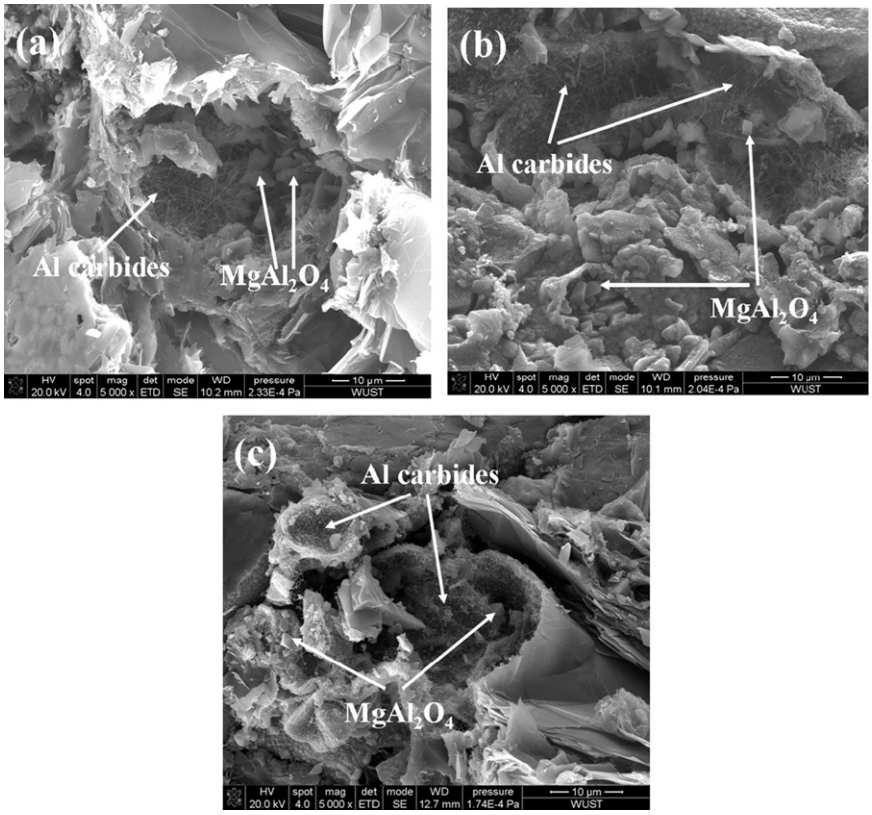


Fig. 4. SEM micrographs of MgO–C refractory specimens (a) S-FG, (b) S-GONs and (c) S-EG fired at 1000 °C.

FG. The highest CMOR and FM values achieved at a firing temperature of 1400 °C were for the specimen S-EG, which were 12.35 MPa and 2824 MPa, respectively.

Fig. 6 shows the force–displacement curves of MgO–C refractory specimens treated at 200 °C, 1000 °C and 1400 °C. It was not difficult to find that the changes of force and displacement had the similar tendency with CMOR and FM of the specimens, i.e. a larger force and displacement corresponded to a higher CMOR and FM. It can be seen that the displacement for the specimens S-GONs and S-EG was larger than for the specimen S-FG irrespective of the treating temperature used. Moreover, the specimen S-EG showed the highest displacement after treatment at all the temperatures.

### 3.4. The thermal shock resistance of MgO–C refractory specimens

The residual CMOR and strength ratio after 5 thermal shock test cycles are shown in Table 4. After the thermal shock tests, the specimen S-EG showed the highest residual CMOR (4.79 MPa) compared to the other two compositions, although higher CMOR values had higher strength loss for the specimen S-EG, similar to the specimen S-GONs. As shown in the SEM micrographs (Fig. 5), the microstructure of the specimen containing EGs and GONs featured the interlocking network of laminated AlN phase and the pulling-out of EGs, which contributed to better thermal shock resistance.

### 3.5. Discussion

Based on the results presented above, it may be concluded that the phase composition and microstructure of the MgO–C refractories studied were influenced by the firing temperature and addition of EGs. At 1000 °C, aluminum carbide ($Al_4C_3$) existed in the form of whiskers [reactions (1) and (2)] (Fig. 4), which transferred almost completely to the lamellate AlN at 1400 °C [reactions (3) and (4)] (Fig. 5). The formation of cuboidal spinel might be based on reactions (5)–(11) (Figs. 4 and 5). Although SiC whiskers or particles could not be identified in SEM micrographs for the specimens of all the compositions, XRD analysis demonstrated the existence of SiC (Fig. 2b). The occurrence was attributed to the reactions (12)–(15).

$$4Al(l,g)+3C(s)=Al_4C_3(s) \quad (1)$$

$$8Al(l,g)+6CO(g)=2Al_4C_3(s)+3O_2(g) \quad (2)$$

$$2Al(l,g)+N_2(g)=2AlN(s) \quad (3)$$

$$Al_4C_3(s)+2N_2(g)=4AlN(s)+3C(s) \quad (4)$$

$$2Al(l,g)+3CO(g)=Al_2O_3(s)+3C(s) \quad (5)$$

$$Al_4C_3(s)+6CO(g)=2Al_2O_3(s)+9C(s) \quad (6)$$

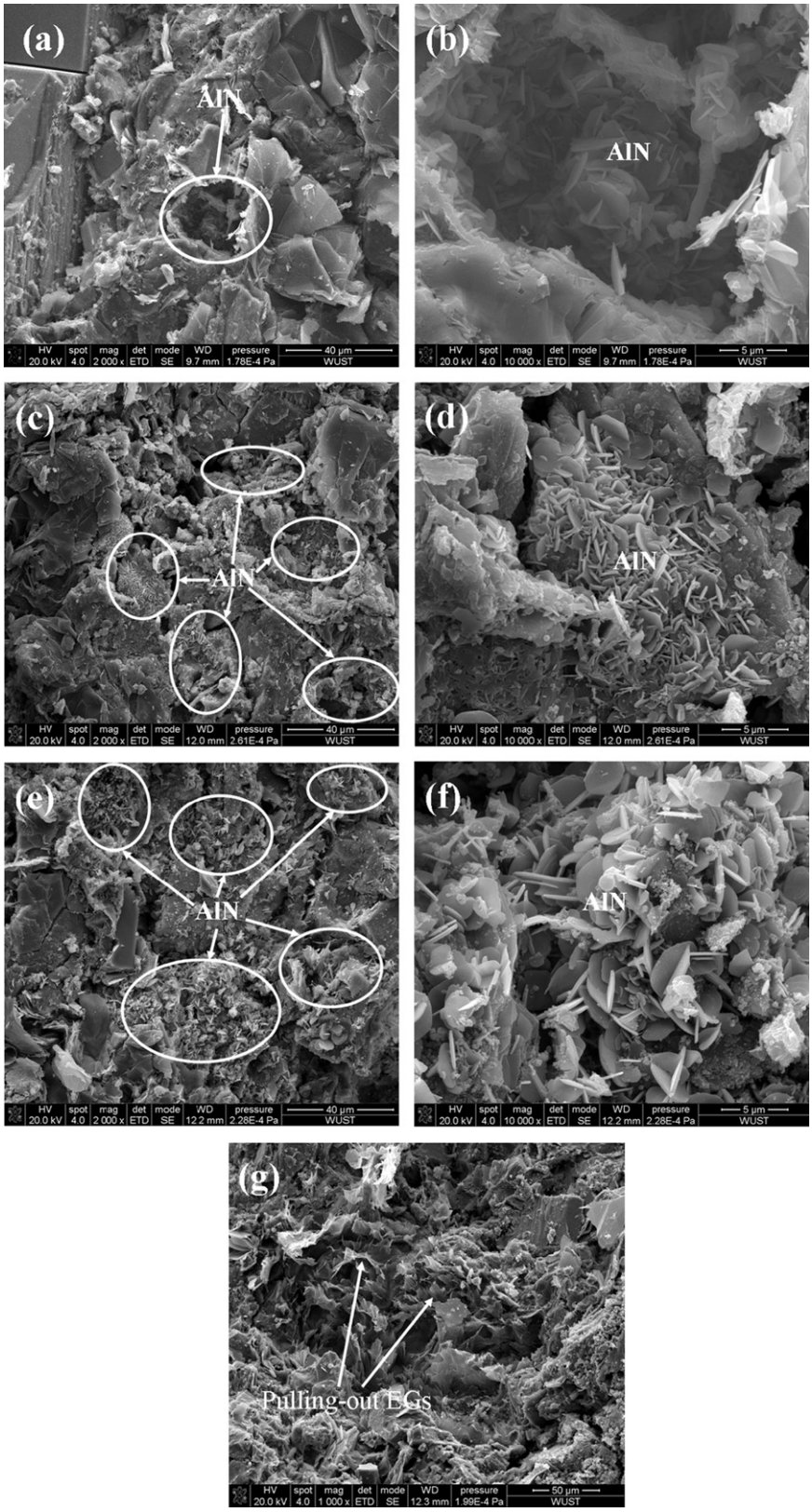


Fig. 5. SEM micrographs of MgO–C refractory specimens (a,b) S-FG, (c,d) S-GONs and (e–g) S-EG fired at 1400 °C.

$$Al_2O_3(s)+MgO(s)=MgAl_2O_4(s) \quad (7)$$

$$Al_4C_3(s)=4Al(g)+3C(s) \quad (8)$$

$$2Al(g)+MgO(s)+3CO(g)=MgAl_2O_4(s)+3C(s) \quad (9)$$

$$MgO(s)+C(s)=Mg(g)+CO(g) \quad (10)$$

$$Mg(g)+2Al(g)+4CO(g) = MgAl_2O_4(s)+4C(s) \quad (11)$$

$$Si(s,g)+C(s) = SiC(s) \quad (12)$$

$$2Si(s,g)+O2(g) = 2SiO(g) \quad (13)$$

Table 2
CMOR and FM of MgO–C refractory specimens treated at various temperatures.

| Temperature (°C) | Index | S-FG | S-GONs | S-EG |
|---|---|---|---|---|
| 200 | CMOR (MPa) | 20.33 | 23.96 | 28.32 |
| | FM (MPa) | 5484 | 5943 | 6515 |
| 1000 | CMOR (MPa) | 6.41 | 7.72 | 6.30 |
| | FM (MPa) | 2137 | 2261 | 1881 |
| 1400 | CMOR (MPa) | 10.02 | 10.97 | 12.35 |
| | FM (MPa) | 2647 | 2758 | 2824 |

Table 3
BD and AP of MgO–C refractory specimens treated at various temperatures.

| Temperature (°C) | Index | S-FG | S-GONs | S-EG |
|---|---|---|---|---|
| 200 | AP (%) | 7.6 | 6.4 | 5.9 |
| | BD ($g\,cm^{-3}$) | 2.96 | 3.00 | 3.02 |
| 1000 | AP (%) | 12.7 | 11.8 | 13.3 |
| | BD ($g\,cm^{-3}$) | 2.93 | 2.95 | 2.92 |
| 1400 | AP (%) | 12.3 | 12.0 | 12.1 |
| | BD ($g\,cm^{-3}$) | 2.94 | 2.96 | 2.96 |

$$SiO(g)+2C(s) = SiC(s)+CO(g) \quad (14)$$

$$SiO(g)+3CO(g) = SiC(s)+2CO2(g) \quad (15)$$

For the specimens containing EGs and GONs, it may be deduced that the EGs and GONs promoted the in situ formation of ceramic phases, especially the formation of aluminum carbides whiskers and lamellate AlN at 1000 °C and 1400 °C, respectively. Difference in the microstructure of specimens fired at different temperatures may be ascribed to the higher activity of small sized EGs and GONs compared with flaky graphite [35,36]; the small sized EGs and GONs decreased the partial pressure of oxygen in the matrix, which further accelerated the formation of ceramic phases in the matrix.

For the specimens fired at 1000 °C, the one with the composition S-GONs had the highest CMOR, which was due to the capability of GONs to promote the formation of aluminum carbides whiskers in the matrix (Fig. 4). For the specimens with the compositions S-EG and S-GONs fired at 1400 °C, more AlN phase formed in the matrix

Table 4
The CMOR change of MgO–C refractory specimens fired at 1400 °C after 5 thermal shocks.

| | S-FG | S-GONS | S-EG |
|---|---|---|---|
| CMOR (MPa) | 10.02 | 10.97 | 12.35 |
| $CMOR_{TS}$ (MPa) | 3.75 | 4.56 | 4.79 |
| The residual strength ratio (5TS) (%) | 37.43 | 41.57 | 38.79 |

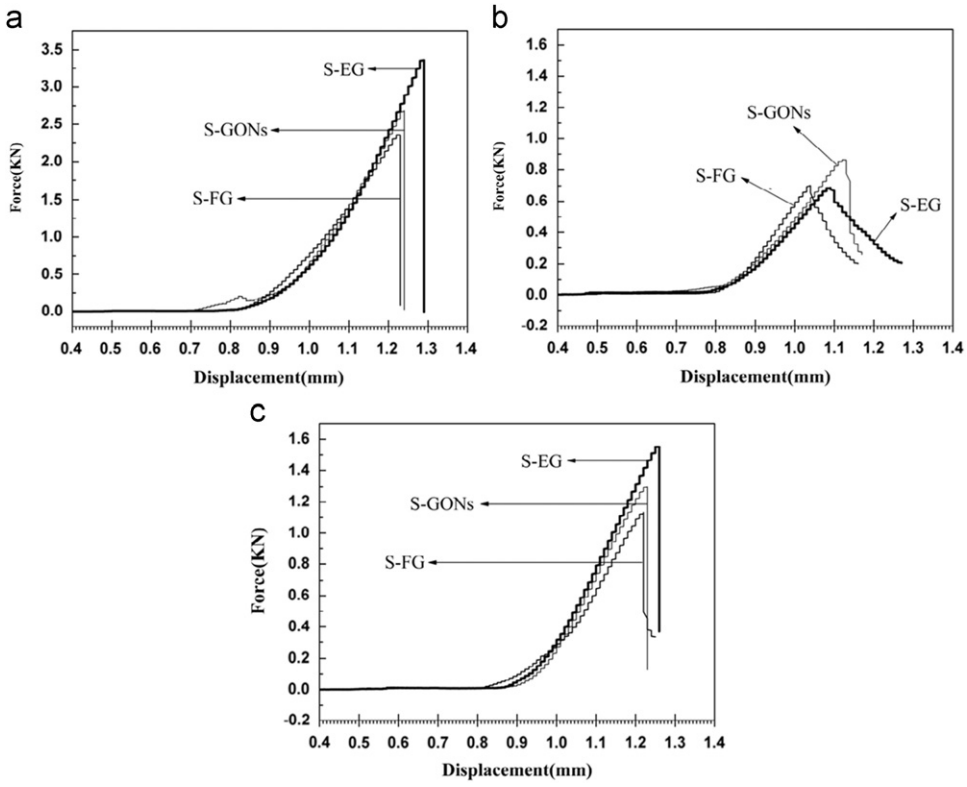


Fig. 6. Force–displacement curves of MgO–C refractory specimens treated at 200 °C (a), 1000 °C (b) and 1400 °C (c).

with interlocking grain morphologies, which provided better mechanical properties. In addition, the fracture and pulling-out of EGs in the matrix toughened and strengthened MgO–C specimens, as also observed in studies by other investigations [31,37,38].

## 4. Conclusions

The EGs were prepared and used to prepare MgO–C refractory specimens. The microstructures were analyzed and mechanical properties were measured for the specimens after heat treatment at different temperatures in a coke bed. The following conclusions can be made with the results obtained:

(1) Adding EGs affected the microstructural evolution of MgO–C refractories during heat treatment. Much more interlocking aluminum carbides whiskers and laminated aluminum nitride phases formed in the matrix of the specimen containing EGs after firing at 1000 °C and 1400 °C, respectively.
(2) The specimens containing EGs exhibited higher strength and higher toughness, which was attributed to the strengthening provided by the formation of much more ceramic phases in the matrix and the toughening facilitated by a mechanism of pulling-out of EGs.

## Acknowledgments

The authors would like to thank the financial support from the National "973" Project of China (2012CB722702), the Natural Science Foundation of China (51002108), the Natural Science Foundation of Hubei Province (2009CDA050) and the programs of the New Century Excellent Talents in University (NCET-10-0137).

## References

[1] S. Tamura, T. Ochiai, S. Takanaga, T. Kanai, H. Nakamura, Nano-tech. refractories-1: the development of the nano structural matrix, in: Proceedings of the UNITECR'03 Congress, Osaka, Japan, 19–22 October, 2003, pp. 517–520.
[2] S. Takanaga, T. Ochiai, S. Tamura, T. Kanai, H. Nakamura, Nano-tech. refractories-2: the application of the nano structural matrix to MgO–C bricks, in: Proceedings of the UNITECR'03 Congress, Osaka, Japan, 19–22 October, 2003, pp. 521–524.
[3] S. Takanaga, Y. Fujiwara, M. Hatta, T. Ochiai, S..Tamura, Nano-tech. refractories-3: development of "MgO-rimmed MgO–C brick", in: Proceedings of the UNITECR'05 Congress, Orlando, USA, 8–11 November, 2005.
[4] Y. Shiratani, T. Yotabun, K. Chihara, T. Ochiai, S. Tamura, Nano-tech. refractories-4: the application of the nano structual matrix to SN plates, in: Proceedings of the UNITECR'05 Congress, Orlando, USA, 8–11 November, 2005.
[5] M. Hatta, S. Takanaga, O. Matsuura, T. Ochiai, S. Tamura, Nano-tech. refractories-5: the application of $B_4C$–C nano particles to MgO–C bricks, in: Proceedings of the UNITECR'07 Congress, Dresden, Germany, 18–21 September, 2007, p. 614.
[6] S. Tamura, Y. Urushibara, O. Matsuura, T. Shin, Nano-tech. refractories-6: observation of the texture after carbonization of nano-tech refractories, in: Proceedings of the UNITECR'07 Congress, Dresden, Germany,18–21 September, 2007, p. 627.
[7] H. Hattanda, T. Yotabun, T. Tsuda, T. Ochiai, S. Tamura, Nano-tech. refractories-7: application of nano structured matrix to SN plates, in: Proceedings of the UNITECR'07 Congress, Dresden, Germany, 18–21 September, 2007, pp. 204–207.
[8] S. Tamura, T. Ochiai, S. Takanaga, T. Kanai, H. Nakamura, Nano-tech. refractories-8: technological philosophy and evolution of nano-tech. refractories, in: Proceedings of the UNITECR'11 Congress, Kyoto, Japan, October 30–November 2, 2011.
[9] H. Yasumitsu, M. Hirashima, O. Matsuura, S. Takanaga, T. Ochiai, S. Tamura, Nano-tech. refractories-9: the basic study on the formation of the nano structured marix in MgO–C bricks, in: Proceedings of the UNITECR'11 Congress, Kyoto, Japan, October 30–November 2, 2011.
[10] M. Tanaka, H. Kamioa, J. Yoshitomi, T. Kayama, S. Hanagiri, K. Goto, Nano-tech. refractories-10: nano-tech. MgO–C bricks for converters to minimize the heat loss, in: Proceedings of the UNITECR'11 Congress, Kyoto, Japan, October 30–November 2, 2011.
[11] H. Hattanda, T. Yotabun, T. Tsuda, H. Tanabe, Nano-tech. refractories-11: the application of nano-technology to AG material for SN plates and carbon bricks for blast furnaces, in: Proceedings of the UNITECR'11 Congress, Kyoto, Japan, October 30–November 2, 2011.
[12] M. Bag, S. Adak, R. Sarkar, Study on low carbon containing MgO–C refractory: use of nano carbon, Ceramics International 38 (2012) 2339–2346.
[13] M.M.J. Treacy, T.W. Ebbesen, J.M. Gibson, Exceptionally high Young's modulus observed for individual carbon nanotube, Nature 381 (1996) 678–680.
[14] M.F. Yu, O. Lourie, M.J. Dyer, K. Moloni, T.F. Kelly, Strength and breaking mechanism of multiwalled carbon nanotubes under tensile load, Science 287 (2000) 637–640.
[15] Y. Matsuo, M. Tanaka, J. Yoshitomi, S. Yoon, J., Miyawaki, Effect of the carbon nanofiber addition the mechanical properties of MgO–C brick, in: Proceedings of UNITECR'11 Congress, October 30–November 2, Kyoto, Japan, 2011.
[16] M. Luo, Y. Li, S. Jin, S. Sang, L. Zhao, Y. Li, Microstructures and mechanical properties of $Al_2O_3$–C refractories with addition of multi-walled carbon nanotubes, Materials Science and Engineering A 548 (2012) 134–141.
[17] V. Roungos, C.G. Aneziris, Improved thermal shock performance of $Al_2O_3$–C refractories due to nanoscaled additives, Ceramics International 38 (2012) 919–927.
[18] B.Z. Jang, A. Zhamu, Processing of nanographene platelets (NGPs) and NGP nanocomposites: a review, Journal of Materials Science 43 (2008) 5092–5101.
[19] J.R. Potts, D.R. Dreyer, C.W. Bielawski, R.S. Ruoff, Graphene-based polymer nanocomposites, Polymer 52 (2011) 5–25.
[20] R. Sengupta, M. Bhattacharya, S. Bandyopadhyay, A.K. Bhowmick, A review on the mechanical and electrical properties of graphite and modified graphite reinforced polymer composites, Progress in Polymer Science 36 (2011) 638–670.
[21] Y. Fan, L.J. Wang, J.L. Li, S.K. Sun, F. Chen, L.D. Chen, W. Jiang, Preparation and electrical properties of graphene nanosheet/$Al_2O_3$ composites, Carbon 48 (2010) 1743–1749.
[22] P. Kun, O. Tapaszto, F. Weber, C. Balazsi, Determination of structural and mechanical properties of multilayer graphene added silicon nitride-based composites, Ceramics International 38 (2012) 211–216.
[23] K. Wang, Y.F. Wang, Z.J. Fan, J. Yan, T. Wei, Preparation of graphene nanosheet/alumina composites by spark plasma sintering, Materials Research Bulletin 46 (2011) 315–318.
[24] T.B. Zhu, Y.W. Li, M. Luo, S.B. Sang, Q.H. Wang, L. Zhao, Y.B. Li, S.J. Li, Microstructure and mechanical properties of MgO–C refractories containing graphite oxide nanosheets (GONs), Ceramics International (2012).

[25] Y.W. Li, C.G. Aneziris, X.X. Yi, S.L. Jin, N. Li, Formation of dumbbell-shaped β-SiC whiskers for the manufacturing of advanced composite refractories in the system $Al_2O_3$–$ZrO_2$–C, Interceram-Refractory Manual (2005) 20–23.
[26] C.G. Aneziris, U. Klippel, W. Scharfl, V. Stein, Y.W. Li, Functional refractory material design for advanced thermal shock performance due to titania additions, International Journal of Applied Ceramic Technology 4 (6) (2007) 481–489.
[27] C.G. Aneziris, J. Hubalkova, R. Barabas, Microstructure evaluation of MgO–C refractories with $TiO_2$- and Al-additions, Journal of the European Ceramic Society 27 (2007) 73–78.
[28] Y.W. Li, S.B. Sang, B. Tong, S. Ge, H. Peng, J. Li, Effects of microsilica powder on microstructure and their properties of fired alumina–zirconia–carbon slide gates, in: Proceedings of the UNITECR'09 Congress, Salvalar, Brazil, 13–16 October, 2009.
[29] H.B. Fan, Y.W. Li, S.B. Sang, Microstructures and mechanical properties of $Al_2O_3$–C refractories with silicon additive using different carbon sources, Materials Science and Engineering A 528 (2011) 3177–3185.
[30] H.B. Fan, Y.W. Li, Y.P. Huang, S.B. Sang, Y.B. Li, L. Zhao, Microstructures and mechanical properties of $Al_2O_3$–$ZrO_2$–C refractories using silicon, microsilica or their combination as additive, Materials Science and Engineering A 545 (2012) 148–154.
[31] S. Hayashi, H. Takahashi, A. Watanabe, A. Osaka, Y. Miura, Dependence of mechanical properties of MgO–C bricks on graphite content, Journal of the Ceramic Society of Japan 102 (1) (1994) 23–28.
[32] J.H. Li, L.L. Feng, Z.X. Jia, Preparation of expanded graphite with 160 μm mesh of fine flake graphite, Materials Letters 60 (2006) 746–749.
[33] T. Wei, Z.J. Fan, G.L. Luo, C. Zheng, D.S. Xie, A rapid and efficient method to prepare exfoliated graphite by microwave irradiation, Carbon 47 (2008) 337–339.
[34] S. Zhang, N.J. Marriott, W.E. Lee, Thermochemistry and microstructures of MgO–C refractories containing various antioxidants, Journal of the European Ceramic Society 21 (2001) 1037–1047.
[35] J.H. Han, K.W. Cho, K.H. Lee, H. Kim, Porous graphite matrix for chemical heat pumps, Carbon 36 (12) (1998) 1801–1810.
[36] J.G. Zhao, Q.G. Guo, J.L. Shi, L. Liu, J.S. Jia, Y.C. Liu, H.Q. Wang, Carbon nanotube growth in the pores of expanded graphite by chemical vapor deposition, Carbon 47 (2009) 1747–1751.
[37] J. Lee, I. Bae, Y. Cho, C. Um, Development of low-carbon MgO–C bricks for the RH degasser, in: Proceedings of the 53rd International Colloquium on Refractories, Aachen, Germany, 8–9 September, 2010 pp. 159–162.
[38] G.X. Yin, B. Pan, X.K. Gao, J.D. Wang, Z.G. Yu, Influence of graphite type on properties of ultra-low carbon MgO–CaO–C brick, Refractories 44 (5) (2010) 355–358 in Chinese.